Computer Assisted Proofs of existence of Fiberwise Hyperbolic Invariant Tori in skew products over rigid rotations

Jordi-Lluís Figueras[*‡] Àlex Haro[†‡]

November 18, 2010

Abstract

We present a methodology to perform Computer Assisted Proofs for the existence and (local) uniqueness of Fiberwise Hyperbolic Invariant Tori in skew product systems over rotations. The theoretical basis is a tailored version of the Newton-Kantorovich theorem for the functional equations describing the invariance of tori and their stable and unstable subbundles. The computational tools allow the rigorous manipulation of truncated Fourier series, which parametrize the tori and their subbundles used in the validations. Our methodology exploits the special form of these dynamical systems, and it is based on the results exposed on the papers by Haro and de la Llave, 2006, 2007. We apply these techniques to two scenarios where the invariant tori are on the verge of hyperbolicity breakdown.

1 Overview

The goal of this paper is to present a methodology to perform Computer Assisted Proofs (CAPs) for the existence and (local) uniqueness of Fiberwise Hyperbolic Invariant Tori (FHIT) in skew product systems over rigid rotations. FHIT are invariant tori whose linearized normal dynamics is uniformly hyperbolic (i.e., exponentially dichotomic) [14]. These are Normally Hyperbolic Invariant Manifolds (NHIM) [11, 18]. The dynamical characterization leads to a functional equation for the invariance condition of a torus that fits in the framework of the Newton-Kantorovich theorem. This theorem is the theoretical core for the validation algorithms employed in this paper.

This framework leads to a validation theorem [13], see theorem 2.4, that exploits the special skew product form of the dynamical system. It is remarkable that this theorem satisfies *a posteriori* bounds. Hence, from an approximately invariant torus (e.g. one that has been computed numerically [15]) that satisfies a hyperbolicity assumption, we can conclude that there exists a unique invariant torus nearby. Moreover, we provide upper bounds for the distance between both tori which can be thought as a measure of the error. The validation algorithm presented in this paper rigorously checks these upper bounds. An alternative topological method to validate existence of invariant sets of normally hyperbolic type have been considered in [5], which is based on the method of covering relations [32]. These methods work for more general dynamical systems but can not be used to prove (local) uniqueness of the invariant sets.

[*]Departament de Matemàtica Aplicada i Anàlisi, Universitat de Barcelona, Gran Via 585. 08007 Barcelona. Spain.

[†]*E-mail adress,* J-Ll Figueras: **figueras@maia.ub.es**

[‡]*E-mail adress,* Àlex Haro: **alex@maia.ub.es**

[§]The first author is supported by *Departament d'Universitats, Recerca i Societat de la Informació de la Generalitat de Catalunya* .

[¶]The authors are supported by *Generalitat de Catalunya, CIRIT* n°2009SGR–67 and MCNN, MTM2009-09723.

In order to perform the validations we need to rigorously deal with tori and subbundles. Since parameterizations of these objects are given by periodic functions and the dynamics on the tori are rigid rotations, it is natural to encode them using Fourier series. (Other base manifold or base dynamics could require types of approximations.) The Fourier model we use to manage rigorously with Fourier series is a trigonometric polynomial with interval coefficients plus an interval error. This has been implemented using a `C++` library to manipulate Fourier models together with the rigorous interval library `FILIB++ Interval Library`, see [24]. We emphasize that suitable Fourier and Lindstedt (Fourier-Taylor) models are ubiquitous in computer aided proofs in KAM theory and renormalization theory [6, 9, 10, 21, 22, 25].

We have applied our methodology to study two challenging scenarios where tori are about to break in non-smooth bifurcations. The first case we study is a non-smooth breakdown of a saddle invariant torus, described in [15, 12], for the quasiperiodically driven standard map. Here, the stable and unstable bundles of a saddle torus approach each other in a complex way. In other words, their projections show the typical collision mechanism of creation of Strange Nonchaotic Attractors (SNA) observed, e.g. in the Harper map [16, 20]. Moreover, the corresponding Lyapunov multipliers are away from 1. We report this mechanism for a quasiperiodically forced standard map, and prove the existence of the saddle torus up to a bound. This bound is at a relative distance less than $4.3 \cdot 10^{-7}$ than the estimated value of the breakdown. In this example, around 30000 Fourier modes were necessary to obtain accurate approximations of the invariant torus and, more crucially, its invariant bundles.

The second scenario examined is the so called Heagy-Hammel route [17]. This is a period 2 attracting torus (appeared in a period doubling bifurcation) that collides with its companion repelling torus, producing a SNA. This situation has been observed in numerical experiments on a quasiperiodically driven logistic map, a noninvertible one. Remarkably, the role of noninvertibility in global bifurcations was already noted in [1, 2]. Noninvertibility is also a drawback in rigorous numerical computations, since it implies that the linear dynamics around the torus can not be reduced to constant coefficients. We overcome this problem and prove that the period 2 attracting torus exist up to a specific bound. This is the relative distance which is less than $7.3 \cdot 10^{-4}$ of the estimated value of the breakdown.

We emphasize that, in both examples, we study what happens *before* the non-smooth bifurcations, in a reliable domain of parameters where we prove that smooth invariant tori exists. Accurate numerical approximations of the invariant objects are crucial for the computer assisted proofs of their existence.

All the validations presented here have been tested with several types of computers working under several operating systems, although we just report the results obtained with a machine `Intel(R) Core(TM)2 Quad CPU Q9550 @ 2.83GHz` working under `Debian`, using one of the processors.

Organization of the paper In section §2 we summarize some basic notions on FHIT on skew products, and the theoretical framework necessary for the computer assisted proofs. In section §3 we present the Fourier models and the implementation of the validation algorithms. Sections §4 and §5 report several examples of rigorous validations.

Notation $\mathbb{R}^n$ denotes the n-dimensional real space, and $e_1, \dots e_n$ represents its unit vectors that form the standard basis. For $i = 1, \dots n$, and $v \in \mathbb{R}^n$, $\pi_i v = v_i$ is the ith component of the vector v. $\mathrm{L}(\mathbb{R}^n; \mathbb{R}^k)$ is the space of linear maps from $\mathbb{R}^n$ to $\mathbb{R}^k$, identified by the set of $k \times n$ matrices. The space of endomorphism of $\mathbb{R}^n$, identified by the set of square $n \times n$ matrices, is $\mathrm{L}(\mathbb{R}^n) = \mathrm{L}(\mathbb{R}^n; \mathbb{R}^n)$, and $\mathrm{GL}(\mathbb{R}^n)$ is its subgroup of automorphisms, i.e. the group of invertible $n \times n$ matrices. I_n represents the $n \times n$ identity matrix. $\mathrm{L}(\mathbb{R}^n, \mathbb{R}^m; \mathbb{R}^k)$ denotes the set of bilinear maps from $\mathbb{R}^n \times \mathbb{R}^m$ to $\mathbb{R}^k$. We also denote $\mathrm{L}^2(\mathbb{R}^n; \mathbb{R}^k) = \mathrm{L}(\mathbb{R}^n, \mathbb{R}^n; \mathbb{R}^k)$, and $\mathrm{L}^2(\mathbb{R}^n) = \mathrm{L}^2(\mathbb{R}^n; \mathbb{R}^n)$, If we are given norms in $\mathbb{R}^n$, $\mathbb{R}^m$, $\mathbb{R}^k$, we consider the induced norms in the spaces of linear maps and bilinear maps previously mentioned. For instance, if we consider the maximum norm $|\cdot|$ in $\mathbb{R}^n$, $\mathbb{R}^m$, $\mathbb{R}^k$,

for $M \in \mathrm{L}(\mathbb{R}^n;\mathbb{R}^k)$ with components $M_{i,j} = \pi_i M e_j$ for $i = 1,\dots k$ and $j = 1,\dots,n$,

$$|M| = \max_i \sum_j |M_{i,j}| \ ,$$

and for $B \in \mathrm{L}(\mathbb{R}^n,\mathbb{R}^m;\mathbb{R}^k)$ with components $B^i_{r,s} = \pi_i B(e_r,e_s)$ for $i = 1,\dots k$, $r = 1,\dots,n$ and $s = 1,\dots,m$, we have

$$|B| = \max_i \sum_{r,s} |B^i_{r,s}| \ .$$

Let $\mathbb{T} = \mathbb{R}/\mathbb{Z}$ be the 1-dimensional torus. (z,θ) denote the coordinates on the trivial bundle $\mathbb{R}^n \times \mathbb{T}$ over $\mathbb{T}$. We assume that the bundle $\mathbb{R}^n \times \mathbb{T}$ is endowed with a Finslered norm, i.e. a norm $|\cdot|_\theta$ on each fiber $\mathbb{R}^n \times \{\theta\}$, that depends continuously on θ. We typically suppress the subindex θ when the fiber is understood, or if the norm does not depend on θ (e.g. we consider the sup norm on each fiber). Finslered norms on the bundles $\mathbb{R}^n \times \mathbb{T}$, $\mathbb{R}^m \times \mathbb{T}$, $\mathbb{R}^k \times \mathbb{T}$ induce Finslered norms in $\mathrm{L}(\mathbb{R}^n;\mathbb{R}^k) \times \mathbb{T}$ and $\mathrm{L}(\mathbb{R}^n,\mathbb{R}^m;\mathbb{R}^k) \times \mathbb{T}$.

A strip in the bundle $\mathbb{R}^n \times \mathbb{T}$ is a set $D \subset \mathbb{R}^n \times \mathbb{T}$ such that for each $\theta \in \mathbb{T}$ the fiber $D_\theta = \{z \in \mathbb{R}^n \mid (z,\theta) \in D\} \subset \mathbb{R}^n$ has non-empty interior. A typical example is $D = U \times \mathbb{T}$, where $U \subset \mathbb{R}^n$ is open.

For a vector space Z and a Finslered norm in the trivial bundle $Z \times \mathbb{T}$ over $\mathbb{T}$, we identify the space of continuous sections of the bundle with the set of continuous functions $\sigma : \mathbb{T} \to Z$, $\mathcal{C}^0(\mathbb{T};Z)$, endowed with the supremum norm $||\sigma||_{\mathcal{C}^0} = \sup_{\theta\in\mathbb{T}} |\sigma(\theta)|_\theta$.

For a map $F\colon \mathbb{R}^n \times \mathbb{T} \to \mathbb{R}^n$, two times differentiable w.r.t. z, $\mathrm{D}_z F(z,\theta)$ and $\mathrm{D}^2_z F(z,\theta)$ denote the first and the second differential of F with respect to z, respectively.

2 Fiberwise Hyperbolic Invariant Tori

In this section we review some definitions and results on Fiberwise Hyperbolic Invariant Tori (FHIT) for skew products over rotations. We further present a tailored version of the Newton-Kantorovich theorem, see theorem 1 in [13], which is the basis for our validation algorithms of existence and local uniqueness of FHIT.

2.1 Definitions and results

A *skew product* over a rotation is a continuous bundle map

$$\begin{array}{rccc} (F,\omega): & \mathbb{R}^n \times \mathbb{T} & \longrightarrow & \mathbb{R}^n \times \mathbb{T} \\ & (z,\theta) & \longrightarrow & (F(z,\theta),\theta+\omega) \end{array} \ , \tag{1}$$

where $F\colon \mathbb{R}^n \times \mathbb{T} \to \mathbb{R}^n$ is continuous and $\omega \in \mathbb{R}$. If $\omega \in \mathbb{R}/\mathbb{Q}$, (F,ω) is a quasiperiodic skew product; otherwise it is periodic. Throughout this paper, we assume that F is $\mathcal{C}^2$ with respect to z.

The graph of a continuous section $K\colon \mathbb{T} \to \mathbb{R}^n$ of the bundle $\mathbb{R}^n \times \mathbb{T}$, $\mathcal{K} = \{(K(\theta),\theta) \,|\, \theta \in \mathbb{T}\}$, is a torus. We often abuse notation and refer to K as a torus, rather than a section or the parametrization of the torus $\mathcal{K}$. If the section K satisfies the functional equation

$$F(K(\theta),\theta) - K(\theta+\omega) = 0 \ , \tag{2}$$

then the torus $\mathcal{K}$ is invariant under (F,ω) and its inner dynamics is the rigid rotation ω.

In functional terms this can be rewritten as follows. Let $\mathcal{T}\colon \mathcal{C}^0(\mathbb{T},\mathbb{R}^n) \to \mathcal{C}^0(\mathbb{T},\mathbb{R}^n)$ be the operator defined as

$$\mathcal{T}(K)(\theta) = F(K(\theta-\omega),\theta-\omega) - K(\theta) \ . \tag{3}$$

K is an invariant torus for (F, ω) if and only if

$$\mathcal{T}(K)(\theta) = 0. \tag{4}$$

A sufficient condition to solve (4) is the invertibility of the corresponding linear operator $\mathrm{D}\mathcal{T}(K) : \mathcal{C}^0(\mathbb{T}, \mathbb{R}^n) \to \mathcal{C}^0(\mathbb{T}, \mathbb{R}^n)$, defined as

$$\mathrm{D}\mathcal{T}(K)\Delta(\theta) = \mathrm{D}_z F(K(\theta - \omega), \theta - \omega)\Delta(\theta - \omega) - \Delta(\theta) \ . \tag{5}$$

The invertibility property of $\mathrm{D}\mathcal{T}(K)$ is strongly related to the hyperbolicity property of the linearized dynamics around K. This is given by the vector bundle map

$$\begin{array}{rccc} (M_K, \omega): & \mathbb{R}^n \times \mathbb{T} & \longrightarrow & \mathbb{R}^n \times \mathbb{T} \\ & (v, \theta) & \longrightarrow & (M_K(\theta)v, \theta + \omega) \end{array} \ , \tag{6}$$

where $M_K \colon \mathbb{T} \to L(\mathbb{R}^n)$ is the *transfer matrix* $M_K(\theta) = \mathrm{D}_z F(K(\theta), \theta)$. We suppress the dependence on K in the notation when it is clear from the context. M is also known as a (linear) *cocycle*.

Define the *transfer operator* $\mathcal{M}$ associated to the torus K as the bounded linear operator $\mathcal{M} : \mathcal{C}^0(\mathbb{T}; \mathbb{R}^n) \to \mathcal{C}^0(\mathbb{T}; \mathbb{R}^n)$ defined as

$$\mathcal{M}(\Delta)(\theta) = M(\theta - \omega)\Delta(\theta - \omega). \tag{7}$$

The relation between the dynamical properties of the linear skew product (M, ω) and the spectral properties of the associated transfer operator $\mathcal{M}$, have been intensively studied in the literature, see e.g. [27, 30, 26, 23, 8]. A key result is the following (see [18] for a more general version).

Theorem 2.1. *Let $(M, \omega) : \mathbb{R}^n \times \mathbb{T} \to \mathbb{R}^n \times \mathbb{T}$ be a linear skew product, and $\mathcal{M} : \mathcal{C}^0(\mathbb{T}; \mathbb{R}^n) \to \mathcal{C}^0(\mathbb{T}; \mathbb{R}^n)$ its associated transfer operator. The following two properties are equivalent:*

(a) *$\mathcal{M}$ is a hyperbolic operator, that is, its spectrum has empty intersection with the unit circle of the complex plane;*

(b) *(M, ω) is uniformly hyperbolic, that is, there exists a continuous decomposition of the vector bundle $\mathbb{R}^n \times \mathbb{T}$ in a Whitney sum $\mathcal{S} \oplus \mathcal{U}$ of two invariant bundles $\mathcal{S}$ and $\mathcal{U}$, such that M restricted to $\mathcal{U}$ is invertible, and there exists constants $C > 0$ and $0 < \lambda < 1$ such that*

- *If $(v, \theta) \in \mathcal{S}$ then $|M(\theta + (l-1)\omega) \cdots M(\theta)v| \leq C\lambda^l |v|$ for all $l \geq 0$;*
- *If $(v, \theta) \in \mathcal{U}$ then $|M(\theta + l\omega)^{-1} \cdots M(\theta - \omega)^{-1} v| \leq C\lambda^{-l}|v|$ for all $l \leq 0$.*

We emphasize that, since $\mathrm{D}\mathcal{T}(K) = \mathcal{M}_K - \mathcal{I}$, the hyperbolicity property of the transfer operator $\mathcal{M}_K$ implies the invertibility of $\mathrm{D}\mathcal{T}(K)$ and hence, the applicability of Newton method. Invariant tori satisfying these hyperbolicity properties are the main object of this paper.

Definition 2.2. *A fiberwise hyperbolic invariant torus (FHIT for short) of the system (1) is an invariant torus $K : \mathbb{T} \to \mathbb{R}^n$, i.e. it satisfies (2), such that its corresponding transfer operator $\mathcal{M}$ is hyperbolic, i.e. its spectrum does not intersect $\{\lambda \in \mathbb{C} : |\lambda| = 1\}$.*

The invariant bundles $\mathcal{S}$ and $\mathcal{U}$ of the associated linear skew product (M_K, ω), see Theorem 2.1, are the stable and the unstable bundles, respectively. If $\mathcal{U}$ is the zero bundle, i.e. the spectrum of $\mathcal{M}_K$ is inside the unit circle, then we say that the torus K is an attractor. If $\mathcal{S}$ is the zero bundle, i.e. the spectrum of $\mathcal{M}_K$ is outside the unit circle, then the torus K is a repellor. Otherwise we will say that the torus K is a saddle.

Here we consider the case where the bundles $\mathcal{S}$ and $\mathcal{U}$ are trivial. This simplifies the computations. In such a scenario, the linear skew product (M_K, ω) is reducible to a block diagonal matrix.

Thus we can define matrix-valued maps $P\colon \mathbb{T} \to GL(\mathbb{R}^n)$, $\Lambda^s\colon \mathbb{T} \to L(\mathbb{R}^{n_s})$ $\Lambda^u\colon \mathbb{T} \to GL(\mathbb{R}^{n_u})$, with $n_s + n_u = n$, such that

$$P(\theta+\omega)^{-1} M_K(\theta) P(\theta) = \begin{pmatrix} \Lambda^s(\theta) & 0 \\ 0 & \Lambda^u(\theta) \end{pmatrix}. \tag{8}$$

In (8), the first n_s columns of P parametrize the stable bundle and the last n_u columns parametrize the unstable bundle. That is, P is an adapted frame to the hyperbolic splitting. Λ^s and Λ^u give the dynamics on the stable and unstable bundles, respectively. An important situation is when we can reduce (M_K, ω) to constants, i.e. Λ is constant. Then we can say that (M_K, ω) (and the torus K) is reducible.

Remark 2.3. *In cases where we can decompose the trivial bundle $\mathbb{R}^n \times \mathbb{T}$ in a Whitney sum of invariant subbundles of rank 1, i.e. $\mathbb{R}^n \times \mathbb{T} = E^1 \oplus \cdots \oplus E^n$, then we can reduce M_K to a diagonal matrix by using a suitable matrix-valued map P defined from the double covering of $\mathbb{T} = \mathbb{R}/\mathbb{Z}$, $\mathbb{R}/2\mathbb{Z}$. Hence, non-orientability of rank 1 subbundles can easily be overcome with the double covering trick. See [15] for examples of computation of invariant tori with non-orientable bundles.*

2.2 A validation theorem

In previous subsection we have seen the relation between hyperbolicity and the implementability of Newton method. From theorem 1 in [13], the Newton method for finding FHIT converges quadratically, provided that the initial approximations of the torus and its invariant bundles are fairly accurate. The following is a reformulation of such a theorem.

Theorem 2.4. *Let $\mathbb{R}^n \times \mathbb{T}$ be the trivial bundle over $\mathbb{T}$, endowed with the Finslered norm given by the maximum norm on each fiber. Let $F\colon D \subset \mathbb{R}^n \times \mathbb{T} \to \mathbb{R}^n$ be a continuous map defined in an open strip D, $\mathcal{C}^2$ with respect to z, and $\omega \in \mathbb{R}$, defining the skew product $(F, \omega) : D \to \mathbb{R}^n \times \mathbb{T}$.*

Assume we are given:

1.1) *a continuous parametrization $K\colon \mathbb{T} \to \mathbb{R}^n$ of a torus $\mathcal{K} \subset D$;*

1.2) *two continuous matrix-valued maps $P_1, P_2\colon \mathbb{T} \to \mathrm{L}(\mathbb{R}^n)$;*

1.3) *a continuous block diagonal matrix-valued map $\Lambda\colon \mathbb{T} \to \mathrm{L}(\mathbb{R}^n)$, $\Lambda(\theta) = \operatorname{diag}(\Lambda^s(\theta), \Lambda^u(\theta))$, where $\Lambda^s\colon \mathbb{T} \to \mathrm{L}(\mathbb{R}^{n_s})$ and $\Lambda^u\colon \mathbb{T} \to \mathrm{GL}(\mathbb{R}^{n_u})$, with $n = n_s + n_u$.*

Let $\rho, \sigma, \tau, \lambda, \hat{\lambda}$ be positive constants such that:

2.1) *For each $\theta \in \mathbb{T}$, $R(\theta) = P_2(\theta+\omega)\left(F(K(\theta), \theta) - K(\theta+\omega)\right) \in \mathbb{R}^n$ satisfies $|R(\theta)| \le \rho$;*

2.2) *For each $\theta \in \mathbb{T}$, $S(\theta) = P_2(\theta+\omega)\mathrm{D}F(K(\theta), \theta)P_1(\theta) - \Lambda(\theta) \in \mathrm{L}(\mathbb{R}^n)$ satisfies $|S(\theta)| \le \sigma$;*

2.3) *For each $\theta \in \mathbb{T}$, $T(\theta) = P_2(\theta)P_1(\theta) - \mathrm{I}_n \in \mathrm{L}(\mathbb{R}^n)$ satisfies $|T(\theta)| \le \tau$;*

2.4) *For each $\theta \in \mathbb{T}$, $\max\left(|\Lambda^s(\theta)|, |\Lambda^u(\theta)^{-1}|\right) \le \lambda$, $|\Lambda(\theta)| \le \hat{\lambda}$;*

and assume that

2.5) $\lambda + \sigma + \tau < 1$.

Given a positive constant r, let b, h be positive constants such that:

3.1) *For each $(z, \theta) \in \mathbb{R}^n \times \mathbb{T}$ with $z = K(\theta) + P_1(\theta)v$ and $|v| \le r$, then $(z, \theta) \in D$ and $B(z, \theta) = P_2(\theta+\omega)\mathrm{D}_z^2 F(z, \theta)\left[P_1(\theta)\cdot, P_1(\theta)\cdot\right] \in L^2(\mathbb{R}^n)$ satisfies $|B(z, \theta)| \le b$;*

3.2) $(1 - \lambda - \sigma - \tau)^{-2} b\rho \le h$;

and assume that

3.3) $h < \frac{1}{2}$.

Assume also that the positive constants r_0, r_1 satisfy:

4.1) $(1-\lambda-\sigma-\tau)(1-\sqrt{1-2h})b^{-1} \leq r_0 \leq r$;

4.2) $r_1 \leq (1-\lambda-\sigma-\tau)(1+\sqrt{1-2h})b^{-1}$ *and* $r_1 \leq r$.

Then, there exists a unique continuous map $K_*\colon \mathbb{T} \to \mathbb{R}^n$ such that, for each $\theta \in \mathbb{T}$:

a.1) $F(K_*(\theta),\theta) - K_*(\theta+\omega) = 0$;

a.2) $|P_1^{-1}(\theta)\,(K_*(\theta) - K(\theta))\,| \leq r_1$.

Moreover:

a.3) $|P_1^{-1}(\theta)\,(K_*(\theta) - K(\theta))\,| \leq r_0$.

If, moreover, the positive constants σ', μ satisfy:

5.1) $(1-\tau)^{-1}(br_0 + \sigma + \hat{\lambda}\tau) \leq \sigma'$;

5.2) $\lambda(1-\lambda^2)^{-1}\sigma' \leq \mu < \frac{1}{4}$;

then there exist continuous matrix-valued maps $P_*\colon \mathbb{T} \to \mathrm{GL}(\mathbb{R}^n)$, $\Lambda_*\colon \mathbb{T} \to \mathrm{L}(\mathbb{R}^n)$, with $\Lambda_*(\theta) = \mathrm{diag}\,(\Lambda_*^s(\theta), \Lambda_*^u(\theta))$, where $\Lambda_*^s\colon \mathbb{T} \to \mathrm{L}(\mathbb{R}^{n_s})$ and $\Lambda_*^u\colon \mathbb{T} \to \mathrm{GL}(\mathbb{R}^{n_u})$, such that, for each $\theta \in \mathbb{T}$:

b.1) $P_*(\theta+\omega)^{-1}\mathrm{D}_z F(K_*(\theta),\theta)P_*(\theta) - \Lambda_*(\theta) = 0$;

b.2) $|P_1(\theta)^{-1}(P_*(\theta) - P_1(\theta))| \leq \frac{\mu}{\sqrt{1-4\mu}}$;

b.3) $|\Lambda_*(\theta) - \Lambda(\theta)| \leq \left(1 + \frac{\mu}{\sqrt{1-4\mu}}\right)\sigma'$.

Remark 2.5. *As a consequence of theorem 2.4, K_* parametrizes a FHIT, and the columns of P_* contain frames of its invariant bundles. Moreover, the convergence of the Newton method to K_* from K is quadratic.*

Remark 2.6. *From the results in [14], the torus K_* is as smooth as the map F (including analytic).*

Remark 2.7. *The Finslered norm appearing in theorem 2.4 is the sup norm on each fiber. More general norms can be considered [13], e.g. the Lyapunov metric adapted to the hyperbolic splitting. Instead of considering adapted metrics, theorem 2.4 considers adapted frames.*

Remark 2.8. *The norm of the second differential (in the coordinates of the adapted frame P_1), is bounded by b for all points in the strip*

$$\bar{D}_{P_1}(K,r) = \{(z,\theta) \mid |P_1^{-1}(\theta)(z - K(\theta))| \leq r\}.$$

This bound b (and subsequently h) depends obviously on the radius r of the strip. A first choice is taking $2(1-\lambda-\sigma-\tau)^{-1}\rho \leq r$, that assures (if $h < \frac{1}{2}$) that $r_0 \leq r$, assumption that appears in 4.3*). We can also tune r in order to improve (making smaller) the* error radius r_0 *and the improving (making bigger) the* uniqueness radius r_1.

Remark 2.9. *One can state a similar theorem using norms with higher regularities (e.g. $\mathcal{C}^r$, Sobolev, analytic). In this paper we have only considered (and implemented) validations using $\mathcal{C}^0$ norms. Hence, although the FHIT K_* is as smooth as the skew product and the bundles are as smooth as its differential, we only measure the distance of the invariant objects to the approximately invariant objects using $\mathcal{C}^0$ norms. We plan to comeback to this problem in the future.*

Remark 2.10. *Theorem 2.4 works also if $\mathbb{T}$ is replaced by a general compact metric space, and $\omega : \mathbb{T} \to \mathbb{T}$ is replaced by a general homeomorphism. However, the fiberwise hyperbolic invariant graph K_* obtained will be in general less regular than F.*

3 Implementation of the validation algorithm

In this section we explain implementation issues of computer validations of FHIT in skew products over rotations, based on Theorem 2.4. Since the base manifold of the skew product is a torus, and the base dynamics is a rotation, we use Fourier polynomials to approximate the periodic functions giving the components of the approximate invariant tori and bundles of the input data. We emphasize that other dynamics and/or other manifolds would lead to other types of approximations, such as simplices, splines, etc.

The core of the implementation is a set of routines to manage Fourier polynomials that approximate periodic functions. This provides rigorous bounds of the coefficients and the tails. These are what we refer as the Fourier models (see [29] for descriptions of Taylor models, and [21, 22] for several Fourier and Fourier-Taylor models).

The validating computer program has to verify, from an approximately invariant torus and approximately invariant stable and unstable bundles (e.g. computed numerically or using perturbative arguments), all the hypothesis of Theorem 2.4. Notice that the checking has to be done only once. Since we will apply the computer programs in situations in which tori are about to break, see sections §4 and §5, we prioritize the accuracy over the speed.

3.1 Fourier models

Here we detail the implementation of Fourier models, assuming the reader is familiar with interval computations [28]. In what follows, when we refer to interval we mean a compact interval. Given an interval $J = [a, b]$, we denote $J^- = a, J^+ = b$. The modulus of an interval is $|J| = \max(|J^-|, |J^+|)$. Following the standard findings in the literature, the result of an operation with intervals is an interval that encloses the result. This is what one can do when implementing interval operations in a computer.

Definition 3.1. *A (one dimensional, real) Fourier model of order $m \geq 0$ is a couple $\hat{G} = (G(\theta), R)$, where*

$$G(\theta) = A_0 + \sum_{k=1}^{m} \left(A_k \cos(2\pi k\theta) + B_k \sin(2\pi k\theta) \right)$$

is a trigonometric polynomial with interval coefficients $A_0, \ldots, A_m$, $B_1, \ldots B_m$, *and the* reminder $R = R(\hat{G})$ *is an interval. Abusing notation, we denote $B_0 = \{0\}$, and for all $k > m$ we define $A_k = B_k = \{0\}$. We also mean by Fourier model of order -1 as an interval R.*

We say that a continuous function $f \colon \mathbb{T} \to \mathbb{R}$ belongs to the Fourier model $\hat{G}$, denoted $f \in \hat{G}$, if for all $\theta \in \mathbb{T}$, $f(\theta) \in A_0 + \sum_{k=1}^{m} (A_k \cos(2\pi k\theta) + B_k \sin(2\pi k\theta)) + R$.

Let $\hat{G}, \hat{H}$ be two Fourier models. We say that $\hat{G}$ is enclosed by $\hat{H}$, $\hat{G} \subset \hat{H}$, iff for any continuous periodic function $f \colon \mathbb{T} \to \mathbb{R}$, $f \in G$ implies $f \in H$.

Given an interval J, the image of J under the Fourier model $\hat{G}$ is defined as $\hat{G}(J) = G(J) + R(\hat{G})$, where $G(J)$ is the interval image of J under the trigonometric polynomial with interval coefficients G. That is, $\hat{G}(J) = \{f(\theta) \in \mathbb{R} \mid f \in \hat{G}, \theta \in J\}$. The image of $\hat{G}$ is $\hat{G}([0, 1])$. The supremum norm is the non-negative number $||\hat{G}|| = |\hat{G}([0, 1])|$. An upper bound of the supremum norm is the ℓ^1-norm $||\hat{G}||_1 = |A_0| + \sum_{k=1}^{m} (|A_k| + |B_k|) + |R|$.

Remark 3.2. *The computer implementation of $\hat{G}(J)$ obtains an enclosure E of the result, i.e. $\hat{G}(J) \subset E$. In order to avoid large overestimations, specially in cases in which the functions $f \in \hat{G}$ behave wildly, we consider suitable subdivisions $J = \bigcup_{i=1}^{n} J_i$ in subintervals J_i, computing the enclosures E_i of the $\hat{G}(J_i)$.*

Definition 3.3. *Let $\hat{G} = (G(\theta), R)$ be a Fourier model of order m, and $\ell \geq 0$. We define the ℓ-tail of $\hat{G}$ as $\hat{G}_{>\ell} = (G_{>\ell}(\theta), R)$, where $G_{>\ell}(\theta) =$ is the (intervalar) Fourier polynomial $\sum_{k=\ell+1}^{m} (A_k \cos(2\pi k\theta) + B_k \sin(2\pi k\theta))$. We define the ℓ-enclosure of $\hat{G}$ as $\hat{G}_{\leq \ell} = (G_{\leq \ell}, \hat{G}_{>\ell}([0, 1]))$,*

where $G_{\leq \ell}(\theta) = A_0 + \sum_{k=1}^{\ell} \left(A_k \cos(2\pi k\theta) + B_k \sin(2\pi k\theta)\right)$. *Abusing notation,* $\hat{G}_{>-1} = \hat{G}$, $\hat{G}_{\leq -1} = \hat{G}([0,1])$.

Given a d-variable function $\varphi(x_1, \ldots, x_d)$, and d Fourier models $\hat{G}_1, \ldots, \hat{G}_d$, we are interested in computing a Fourier model $\hat{H}$ enclosuring the composition $\varphi \circ \hat{G}$, where $\hat{G} = (\hat{G}_1, \ldots, \hat{G}_d)$. That is, we want that, for all $\theta \in \mathbb{T}$, $\varphi(\hat{G}(\theta)) \subset H(\theta)$. We will consider here the case that φ is elementary (in the Liouville sense), that is we will assume the φ is a combinations of finitely many arithmetic operations and compositions with simple functions (or intrinsic functions [29]) such as the power function, the exponential function or the trigonometric functions.

The arithmetic operations with Fourier models are defined as follows. Addition and subtraction of two Fourier models $\hat{G}$ and $\hat{H}$ is defined componentwise:

$$\hat{G} + \hat{H} = (G(\theta) + H(\theta), R(\hat{G}) + R(\hat{H})) \ , \ \hat{G} - \hat{H} = (G(\theta) - H(\theta), R(\hat{G}) - R(\hat{H})).$$

If J is an interval, we define the multiplication of $\hat{G}$ with J as

$$J \cdot \hat{G} = (JG(\theta), JR).$$

The product of $\hat{G}$ and $\hat{H}$ is

$$\hat{G} \cdot \hat{H} = (G(\theta)H(\theta), G([0,1])R(\hat{H}) + H([0,1])R(\hat{G}) + R(\hat{G})R(\hat{H})).$$

In order to bound the order of the Fourier models through the operations in a computation, we in fact compute enclosures of the products. For instance, if $\hat{G}$ and $\hat{H}$ are two Fourier models of order m, their m-product is the m-enclosure of the product, i.e. $(\hat{G} \cdot \hat{H})_{\leq m}$.

Once we have defined the arithmetic operations with Fourier models, compositions with polynomials are straightforward. If $P(x) = C_0 + C_1 x + C_2 x^2 + \ldots + C_n x^n$ is a polynomial with interval coefficients, we compute the composition $P \circ \hat{G}$ using a Hörner scheme:

$$P(\hat{G}) = C_0 + \hat{G} \cdot \left(C_1 + \hat{G} \cdot \left(C_2 + \cdots + \hat{G} \cdot \left(C_{n-1} + C_n \cdot \hat{G}\right) \cdots\right)\right).$$

Since the order of the composition is n times the order m of $\hat{G}$, we usually substitute each product of Fourier models in the Hörner scheme by the corresponding m-product. Hence, we obtain an enclosure of order m of the composition of $\hat{G}$ with P.

Enclosures of the compositions of Fourier models with simple functions, such as the exponential, power function, logarithm, etc. can be performed with the aid of the corresponding Taylor polynomial approximations (and bounds of the Lagrange errors). We consider here the composition with the sine and cosine functions, which are the ones that appear in our examples.

Given $\ell > 0$, let $S_\ell(x)$, $C_\ell(x)$ be the Taylor polynomials of degree ℓ of the sine and cosine functions, respectively. Let

$$\hat{S}_\ell(x) = S_\ell(x) + \frac{[-1,1]}{(\ell+1)!}x^{l+1} \ , \hat{C}_\ell(x) = C_\ell(x) + \frac{[-1,1]}{(\ell+1)!}x^{l+1}$$

be the corresponding polynomials with Lagrange error bounds. Then, the compositions of (F, ω) with the sine and cosine functions are enclosed in

$$\sin_\ell(\hat{G}) = \sin(A_0) \cdot \hat{C}_\ell(\hat{G}_{>0}) + \cos(A_0) \cdot \hat{S}_\ell(\hat{G}_{>0}) \ ,$$
$$\cos_\ell(\hat{G}) = \cos(A_0) \cdot \hat{C}_\ell(\hat{G}_{>0}) - \sin(A_0) \cdot \hat{S}_\ell(\hat{G}_{>0}) \ ,$$

respectively. In computer implementations, the order ℓ of the Taylor polynomials is chosen such that $\left|\frac{1}{(l+1)!}(\hat{G}_{>0}[0,1])^{l+1}\right|$ is less than a given tolerance. We also use m-products in the intermediate computations.

Another operation used in this paper is the shift of a Fourier model $\hat{G} = (G(\theta), R)$ by an (interval) rotation ω. This is the Fourier model $S_\omega(\hat{G}) = (S(\theta), R)$, with $S(\theta) = A_0 + \sum_{k=1}^{m} (A'_k \cos(2\pi k\theta) + B'_k \sin(2\pi k\theta))$, where

$$A'_k = B_k \cos(2\pi k\omega) - A_k \sin(2\pi k\omega) \ , \ B'_k = A_k \cos(2\pi k\omega) + B_k \sin(2\pi k\omega).$$

Remark 3.4. *For the validation algorithms, we also use vector and matrix Fourier models, that are implemented straightforwardly.*

3.2 Validation of FHIT

Here we show how can be implemented, via Fourier models, theorem 2.4 in order to validate some initial data as a good approximation of a FHIT and its invariant subbundles for a given skew product $(F, \omega) : D \subset \mathbb{R}^n \times \mathbb{T} \to \mathbb{R}^n \times \mathbb{T}$, which is continuous, and $\mathcal{C}^2$ with respect to z.

We assume that F is simple, in the sense that we can effectively compute the enclosures of the components of the compositions of $F(z, \theta)$, $\mathrm{D}_z F(z, \theta)$ and $\mathrm{D}_z^2 F(z, \theta)$ with Fourier models. That is, we can substitute z by a (vector) Fourier model $\hat{K}$, if for each $\theta \in [0, 1]$, $\hat{K}(\theta) \subset D_\theta$) (a fact that can be rigorously checked by using interval arithmetics).

0) Compute, e.g. numerically or using perturbative arguments, the trigonometric polynomial approximations of an invariant torus (K), the adapted frame (P_1) and its inverse (P_2), and the dynamics on the invariant bundles ($\Lambda = \mathrm{diag}(\Lambda^s, \Lambda^u)$).

Fix the order m of the Fourier models throughout the rigorous computations of the validation algorithm. The results at each operation of Fourier models will be m-enclosed.

The validation algorithm mimics the statement of theorem 2.4. Here are the steps:

1) From the input data, derive the Fourier models $\hat{K}$, $\hat{P}_1$, $\hat{P}_2$, $\hat{\Lambda} = (\hat{\Lambda}^s, \hat{\Lambda}^u)$.

2) Compute the upper bounds $\rho, \sigma, \tau, \lambda, \hat{\lambda}$ by enclosing the Fourier models $\hat{R}$, $\hat{S}$, $\hat{T}$, $\hat{\Lambda}^s$, $\hat{\Lambda}^u$, $(\hat{\Lambda}^u)^{-1}$. Check (using interval arithmetics) if $\lambda + \sigma + \tau < 1$. If not, the torus is not validated (and algorithm stops).

3) Given r (for instance, an upper bound of $2(1 - \lambda - \sigma - \tau)^{-1}\rho$, see remark 2.8), compute upper bounds b and h. Since we use maximum norms, we compute the Fourier model $\hat{B} = B(\hat{K} + \hat{P}_1 [-r, r]^n, \cdot)$ of the bilinear map $B(z, \theta)$ for points (z, θ) in the strip $\bar{D}_{P_1}(K, r)$ and, hence, b is an upper bound of the maximum norm of $\hat{B}(\theta)$ for all points in $[0, 1]$. Once we compute h, check (using interval arithmetics) if $h < \frac{1}{2}$. If not, the torus is not validated (and algorithm stops).

4) Compute (an upper bound of) the error radius $r_0 \geq (1 - \lambda - \sigma - \tau)\ (1 - \sqrt{1 - 2h})b^{-1}$ and (a lower bound of) the uniqueness radius $r_1 \leq (1 - \lambda - \sigma - \tau)\ (1 + \sqrt{1 - 2h})b^{-1}$. Check if $r_0 \leq r$. If not, the torus is not validated (and algorithm stops).

   Then, the torus is validated, meaning that there is a unique invariant torus K_* in the strip $\bar{D}_{P_1}(K, r_1)$. Moreover, the torus K_* is contained in the strip $\bar{D}_{P_1}(K, r_0)$.

5) Compute the upper bound of μ and σ' using $\sigma, \tau, \lambda, \hat{\lambda}$. Check if $\mu < \frac{1}{4}$. If not, the normal dynamics of the validated torus is not validated (and algorithm stops). Compute the upper bounds $\frac{\mu}{\sqrt{1-4\mu}} \leq \rho_P$ and $\left(1 + \frac{\mu}{\sqrt{1-4\mu}}\right) \sigma' \leq \rho_\Lambda$.

   Hence, the normal dynamics on the torus and the invariant subbundles are validated: they are at a distance less than ρ_Λ, ρ_P from the ones given by the initial data.

3.3 Validation of a family of FHIT

Here we show the procedure to validate the existence of a family of FHIT of a one parameter family of skew products $(F_t, \omega) : D \subset \mathbb{R}^n \times \mathbb{T} \to \mathbb{R}^n \times \mathbb{T}$, with parameter $t \in [a, b]$.

Consider the interval $[a, b] = I \cup J$, where I and J are closed intervals, and let K_i, $P_{1,i}$, $P_{2,i}$ and Λ_i for $i = I, J$ be the initial data of the validation algorithm for the (interval) skew products (F_i, ω). In order to check that the corresponding validated tori belong to the same family we proceed as follows.

0) Apply the validation algorithm explained in subsection §3.2 to the (interval) skew products (F_i, ω), $i = I, J$. Besides the Fourier models corresponding to the initial data, $\hat{K}_i$, $\hat{P}_{1,i}$, $\hat{P}_{2,i}$ and $\hat{\Lambda}_i$, the validation algorithm produces bounds $\rho_i, \sigma_i, \tau_i, r_{0,i}, r_{1,i}, h_i$.

1) Construct the Fourier model $\hat{E}_{I,J} = \hat{P}_{2,J} \cdot \left(\hat{K}_J - \left(\hat{K}_I + \hat{P}_{1,I} \cdot [-r_{0,I}, r_{0,I}]^n\right)\right)$. Check if

$$\|\hat{E}_{I,J}\| \leq (1 - \tau_J) r_{1,J}. \tag{9}$$

If this holds, the two initial data approximates the same family of FHIT, if not, this family has not been validated.

4 Example 1: computer validations on the verge of the hyperbolicity breakdown of a saddle torus

In this section we report computer validations of existence of saddle tori on the verge of their hyperbolicity breakdown for a quasiperiodically forced standard map. This phenomenon was described in [15, 12] for similar models.

4.1 Two bifurcation scenarios of saddle tori in the quasiperiodically forced standard map

The *quasiperiodically forced standard map* is the map $(F, \omega) : \mathbb{T} \times \mathbb{R} \times \mathbb{T} \to \mathbb{T} \times \mathbb{R} \times \mathbb{T}$ defined as

$$\begin{cases} \bar{x} &= x + \bar{y} \\ \bar{y} &= y - \frac{\kappa}{2\pi} \sin(2\pi x) - \varepsilon \sin(2\pi\theta) \\ \bar{\theta} &= \theta + \omega \end{cases}, \tag{10}$$

where we fix $\omega = \frac{1}{2}(\sqrt{5} - 1)$.

For every $\kappa > 0$, there exist a family $K_\varepsilon(\theta)$ of FHIT (saddle type), with $\varepsilon \in (-\varepsilon_c, \varepsilon_c)$, such that $K_0(\theta) = \left(\frac{1}{2}, 0\right)$. Notice that $K_{-\varepsilon}(\theta) = -K_\varepsilon(\theta)$. An interesting problem is approaching as much as possible the limiting value ε_c, the critical parameter value, and study the obstructions to fiberwise hyperbolicity.

Remark 4.1. *Since* (10) *is area preserving, the product of the Lyapunov multipliers associated to the* 1*-dimensional stable and unstable subbundles is equal to* 1*. Then, by an abuse of notation, we refer the Lyapunov multiplier to the maximal Lyapunov multiplier.*

We have done a numerical exploration and we have found that the bifurcation mechanism around ε_c depends on κ:

- For low values of κ, e.g. $\kappa = 0.3$ with $\varepsilon_c \approx 1.3364054$, there is a smooth bifurcation: the hyperbolicity is broken down because the Lyapunov multiplier goes to 1 as ε goes to ε_c, but the invariant subbundles collide smoothly.

- For high values of κ, e.g. $\kappa = 1.3$ with $\varepsilon_c \approx 1.2352755$, there is a non-smooth bifurcation: the hyperbolicity is broken down because the invariant bundles collide non-uniformly as ε goes to ε_c, and the Lyapunov multiplier stays far from 1.

See figure 1 and figure 2 for numerical examples of both scenarios. These figures show the invariant tori and their invariant bundles, and the graphs of the Lyapunov multiplier and minimum distance between the invariant bundles as a function ε.

Numerical estimate of the breakdown value In both examples, we have computed the invariant tori and their invariant bundles, and estimated the critical values ε_c, using the different Fourier methods of [13] and computing periodic orbits for rational approximations $\frac{p}{q}$ of the rotation number ω. These methods produce similar results. Table 1 reports the results using rational approximations for $\kappa = 1.3$.

p	q	ε_c	Λ_c
610	987	**1.235277**250097	**1.4**17569758833
987	1597	**1.235276**717863	**1.42**7183182503
1597	2584	**1.235275**424968	**1.43**2628905747
2584	4181	**1.235275**700525	**1.43**3722000980
4181	6765	**1.2352755**63425	**1.43**6571048918
6765	10946	**1.2352756**11145	**1.43**6207590892
10946	17711	**1.2352755**32096	**1.43**8434241268
17711	28657	**1.2352755**30445	**1.43**8634421523
28657	46368	**1.23527552**6435	**1.43**8911614742
46368	75025	**1.23527552**7297	**1.43**8984187196
75025	121393	**1.23527552**6916	**1.439**054814648
121393	196418	**1.23527552**7050	**1.439**063207687
196418	317811	**1.2352755267**94	**1.439**115016429
317811	514229	**1.2352755267**94	**1.439**117250462
514229	832040	**1.23527552**6885	**1.439**118021353
832040	1346269	**1.235275526763**	**1.439124**814800
1346269	2178309	**1.235275526763**	**1.439124**666214
2178309	3524578	**1.235275526763**	**1.4391247**23263
3524578	5702887	**1.235275526763**	**1.4391247**01574

Table 1: Critical ε_c where the transition occur and their Lyapunov multiplier Λ_c for each of the partial convergent of the golden mean with denominator less than $6 \cdot 10^6$. $\kappa = 1.3$. The bold digits represent the right digits, with respect to the values obtained for the biggest denominator.

4.2 Computer Validations

In this section we report computer validations of the invariant tori for the non-smooth bifurcation scenario, for $\kappa = 1.3$ with $\varepsilon_c = 1.2352755$. This is a challenging example because the invariant subbundles near the bifurcation are quite wild. Thousands of Fourier modes are needed in order to have good initial data for the validation algorithm.

Remark 4.2. *In the smooth bifurcation scenario, the initial data required in order to get successful validations near the bifurcation value need no more than one hundred Fourier modes. For $\kappa = 0.3$, we have validated the FHIT for $\varepsilon = 1.3364$, which is at a relative distance of $3 \cdot 10^{-4}$ of the estimated bifurcation value $\varepsilon_c \approx 1.3364054$.*

In a first run, we have validated tori K_ε for values of ε in a grid of step size $\leq 10^{-2}$ of the parameter interval $[0, 1.2351]$. Note that the difference between the predicted breakdown value ε_c and the last validation $\varepsilon = 1.2351$ is less than of order $1.8 \cdot 10^{-4}$. The results of this first run are reported in figure 3. We observe that, as ε increases, the upper bounds of the validation algorithm h and r_0, that measure the quality of the approximate invariant torus, increases, while the lower

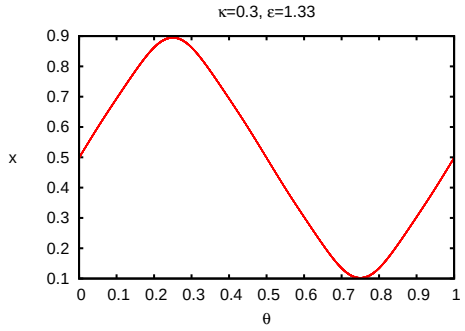

(a) x-coordinate projection of the invariant torus.

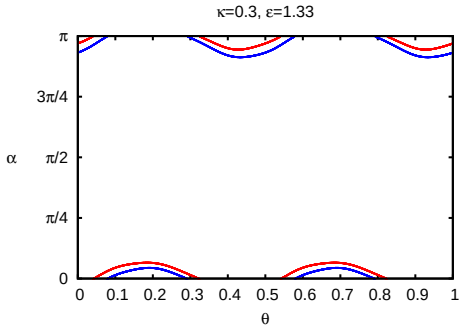

(b) Invariant subbundles represented by their angles with respect to the semiaxis $y = 0$, $x > 0$.

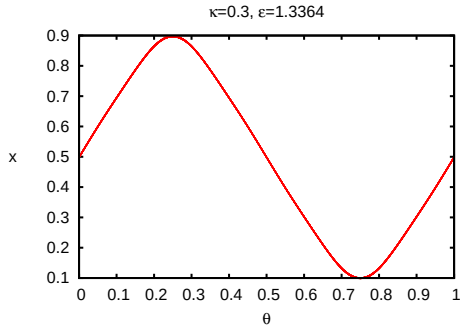

(c) x-coordinate projection of the invariant torus.

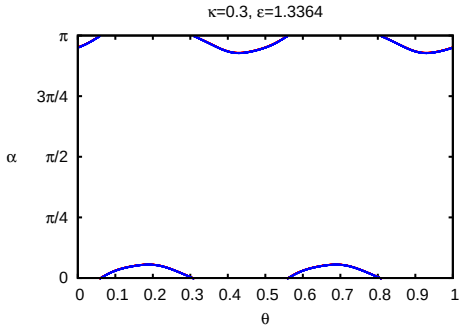

(d) Invariant subbundles represented by their angles with respect to the semiaxis $y = 0$, $x > 0$.

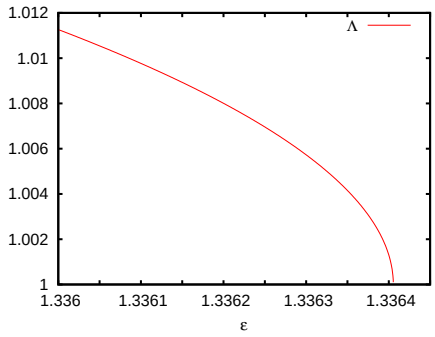

(e) Lyapunov multiplier as a function of ε.

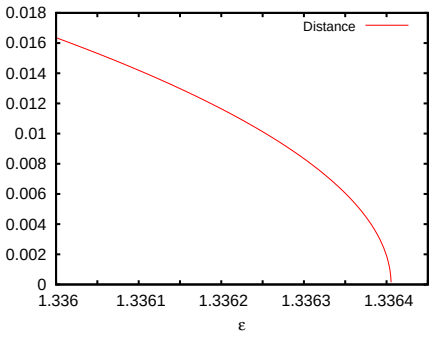

(f) Minimum distance between the invariantsubbundles.

Figure 1: Smooth bifurcation: invariant torus and its subbundles for $\kappa = 0.3$, and the observables measuring hyperbolicity, near the bifurcation value $\varepsilon_c \approx 1.3364054$.

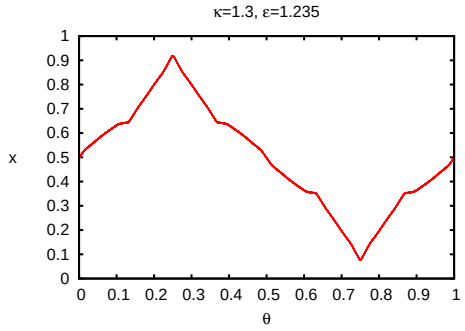

(a) x-coordinate projection of the invariant torus.

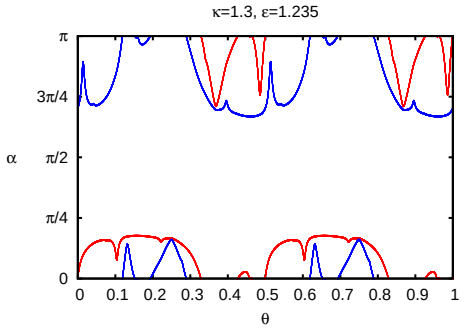

(b) Invariant subbundles represented by their angles with respect to the semiaxis $y = 0$, $x > 0$.

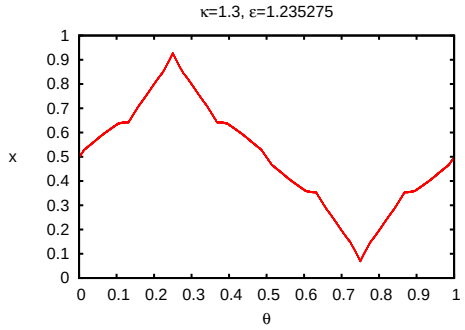

(c) x-coordinate projection of the invariant torus.

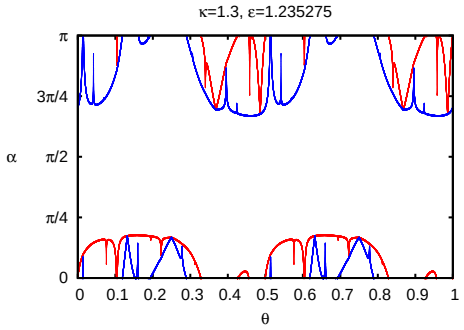

(d) Invariant subbundles represented by their angles with respect to the semiaxis $y = 0$, $x > 0$.

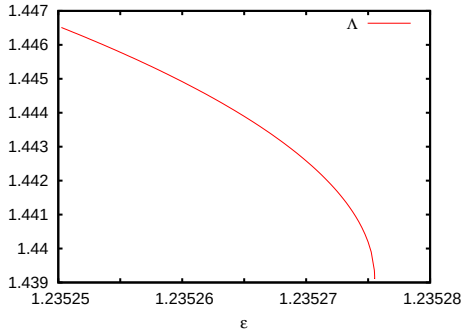

(e) Lyapunov multiplier as a function of ε.

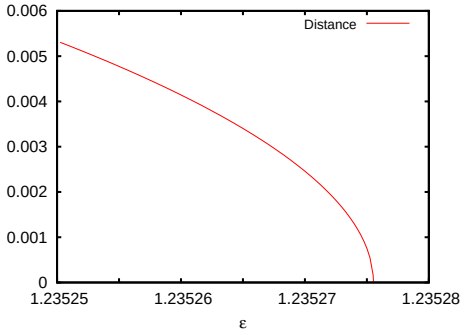

(f) Minimum distance between the invariantsubbundles.

Figure 2: Nonsmooth bifurcation: invariant torus and its subbundles for $\kappa = 1.3$, and the observables measuring hyperbolicity, near the bifurcation value $\varepsilon_c \approx 1.2352755$.

bound of r_1, that measures the size of the uniqueness strip, decreases. We also observe that the upper bounds μ and ρ_Λ, that measure the quality of the approximate invariant bundles, increase. The number of Fourier modes required in the validations increases from 0 to 1280.

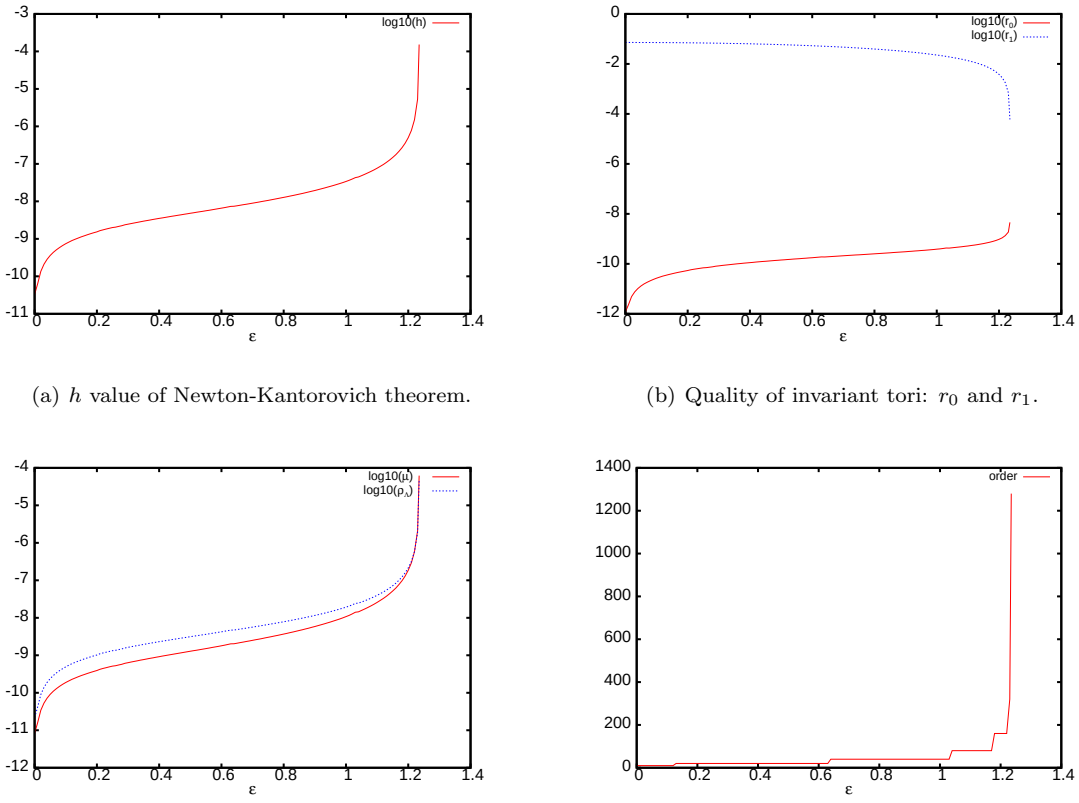

(a) h value of Newton-Kantorovich theorem.

(b) Quality of invariant tori: r_0 and r_1.

(c) Quality of the invariant bundles: μ and ρ_Λ.

(d) Order of Fourier model.

Figure 3: Data output obtained from the validations of the invariant tori and their invariant bundles for $\kappa = 1.3$ with respect to ε. See text for more details.

In order to illustrate the validation algorithm for families of FHIT, we have used it to validate the whole family in the parameter interval $\varepsilon \in [0, 1.073969]$, with Fourier models of order 100. The main problem in order to validate further the family is that the width of the parameter intervals required in the algorithm is too small, of order 10^{-6}.

In a final run, we have validated the initial data for the values $\varepsilon = 1.235270, 1.235273, 1.235275$, with Lyapunov multipliers $\Lambda = 1.442582, 1.441463, 1.440193$, respectively, in order to check the applicability of the validation algorithm extremely close to the non-smooth bifurcation. The output results obtained are shown in table 2. Note that the difference between 1.235275 and the predicted bifurcation value, 1.2352755, is less than $5.3 \cdot 10^{-7}$.

5 Example 2: computer validations for noninvertible skew products

In this section we report computer validations of existence of invariant tori for a noninvertible map, the quasiperiodically driven logistic map. Special emphasis is put on validation of non-reducible

ε	1.235270	1.235273	1.235275
h	2.853269e-03	8.140590e-03	8.928078e-02
r_0	1.302039e-07	2.490723e-07	1.035418e-06
r_1	9.100589e-05	6.069352e-05	2.107294e-05
μ	1.825306e-03	5.188943e-03	3.841927e-02
ρ_Λ	1.370355e-03	3.900239e-03	2.985134e-02
order	5802	7918	27692
time (minutes)	103	154	1094

Table 2: Validation results of invariant tori of the quasiperiodically forced standard map for three ε values near the predicted breakdown. Note that the order of the Fourier models and the time of validation, increase as ε increase.

tori for values close to their breakdown.

5.1 Numerical exploration of invariant curves in the quasiperiodically driven logistic map

The *driven logistic map* is defined as the skew product

$$(F,\omega)\colon \quad \begin{array}{ccc} \mathbb{R}\times\mathbb{T} & \longrightarrow & \mathbb{R}\times\mathbb{T} \\ (z,\theta) & \longrightarrow & (a(1+D\cos(2\pi\theta))z(1-z),\theta+\omega) \end{array} \ , \tag{11}$$

where $\omega=\frac{1}{2}(\sqrt{5}-1)$; and a and D are parameters. We will fix $D=0.1$ and let $a>0$ vary. This map has been the target of several numerical studies, see for example [17, 2], where the authors explore numerically the creation of SNA (Strange Nonchaotic Attractor) via the non-smooth collision of attracting and repellor curves (the Heagy-Hammel route).

In figure 4(a) appears the bifurcation diagram (with respect to a) of the invariant objects, while in figure 4(b) appears the corresponding Lyapunov multipliers. A particularly simple case is the zero-curve $x_a(\theta)=0$, for which the Lyapunov multiplier can be analytically computed (see e.g. [19]): $\Lambda(a)=\frac{a}{2}\left(1+\sqrt{1-D^2}\right)$. Hence, for $D=0.1$, the zero-curve is attracting if $a<2(1+\sqrt{0.99})^{-1}$ and repelling if $a>2(1+\sqrt{0.99})^{-1}\simeq 1.002512$.

Now, let's explain the other invariant curves and their bifurcations, labelled in figure 4(b):

A) $a\in(0,1.002512)$: There is a reducible repellor curve. As $a\to 0$ this curves tends to $\frac{a-1}{a}$, and its Lyapunov multiplier approaches 2. As $a\to 1.002512$ this curves tends to 0.

B) $a\in(1.002512,1.854419)$: There is a reducible attracting curve with positive Lyapunov multiplier ($0<\Lambda<1$). This curve comes from a transcritical bifurcation between the zero-curve $x(\theta)=0$ and the repellor curve of region A.

C) $a\in(1.854419,2.406952)$: There is a non-reducible attracting curve, that is, its transfer matrix vanishes at some points. This curve belongs to the same family of the curve of region A.

D) $a\in(2.406952,3.141875)$: There is a reducible attracting curve with negative Lyapunov multiplier ($-1<\Lambda<0$). This curve also belongs to the same family of curves of regions B and C.

E) $a\in(3.141875,3.271383)$: The attracting curve of region D suffers a period doubling bifurcation. In region E, there is a period 2 attracting curve and a period 1 repellor curve (see figures 5(a) and 5(b) for the corresponding Lyapunov multipliers). For values $a\in(3.141875,3.17496)$ the period 2 attracting curve is reducible and for values $a\in(3.17496,3.271383)$ it is non-reducible.

At a near 3.271383 the period 2 attracting curve collides in a non-smooth way with the repellor curve, bifurcating to a SNA. This is the so-called Heagy-Hammel fractalization route. Figures 6(a) and 6(b) show these invariant objects before and after the bifurcation.

F) $a \in (3.271383, \infty)$: The repellor curve exists for all these values. The SNA *seems to persist* for values in $a \in (3.271383, 3.2746)$, and afterwards its *apparently bifurcates* into a SA (Strange Attractor), with Lyapunov multiplier bigger than 1.

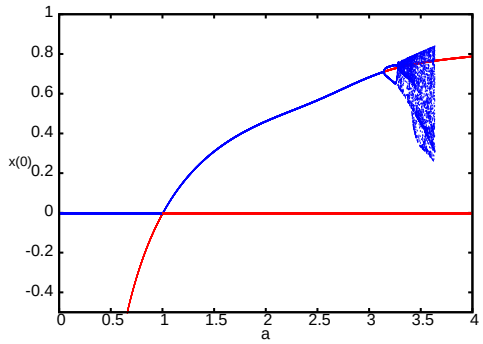

(a) $x(0)$ value of the invariant curves $x(\theta)$ with respect to parameter a. The red color represents a repellor curve and the blue color an attracting object.

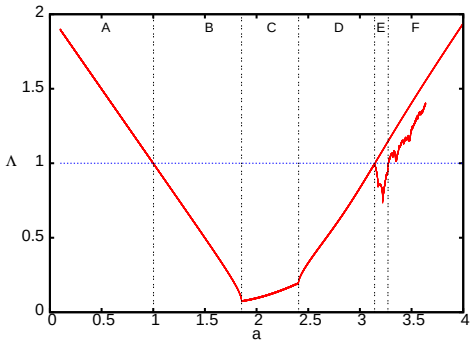

(b) The Lyapunov multiplier of theinvariant curves.

Figure 4: Bifurcation diagram of the invariant curves and their Lyapunov multipliers, with respect to parameter a. See text for further details.

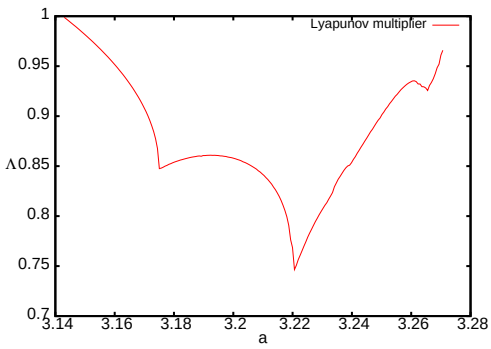

(a) Lyapunov multiplier of the period 2 attracting curve in region E. The peaks correspond to variations of the number of zeroes of the transfer cocycle [19].

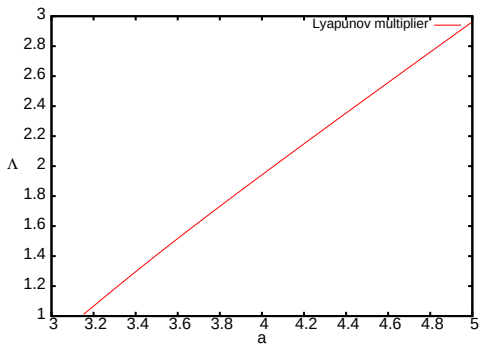

(b) Lyapunov multiplier of the repellor curve in regions E and F. There is no traces of the non-smooth E-F bifurcation of the attracting companion around $a = 3.271$.

Figure 5: Lyapunov multipliers of the invariant and periodic curves, with respect to parameter a.

5.2 Numerical computation of the initial data

In this section, we expose how to compute the initial data K, P_1, P_2, Λ for attracting curves of the noninvertible 1D skew product (F, ω). Similar methods can be applied for repelling curves, by

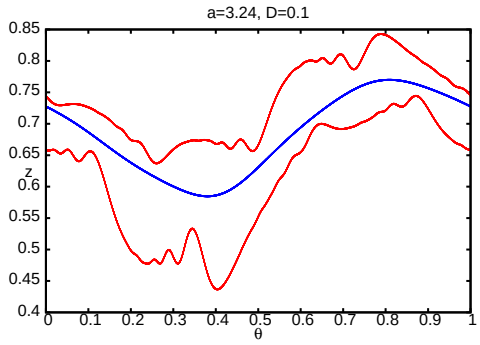

(a) Invariant curves for $a = 3.24$. The red curves is the period 2 attractor, the blue curve is the repellor.

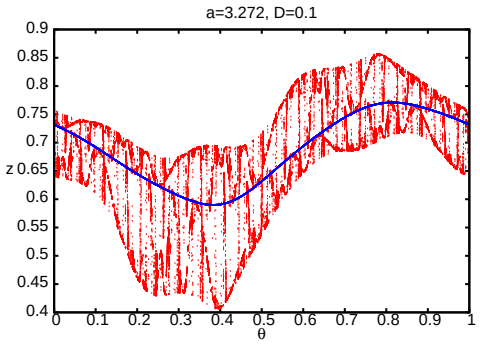

(b) Invariant objects for $a = 3.272$. The red object is the SNA, the blue curve is the repellor.

Figure 6: Graphical representation of the Heagy-Hammel route. See text for further details.

using a right inverse of the map (i.e., one of the branches of the inverse of (F, ω)).

The approximately invariant torus K can be computed using the simple iteration algorithm, since the invariant torus is attracting. The number of iterations needed to have a good approximation depends heavily on the modulus of the Lyapunov multiplier. In our computations, the number of iterations does not exceed 10^{10} simple iterations.

More challenging is the computation of the initial data P_1, P_2, Λ, since even though the transfer matrix M is contracting "in average", it does not mean that it is uniformly contracting for the supremum norm. The condition of invertibility of the transfer matrix plays a key role in this computation. We have consider two methods in order to overcome these computational problems.

Lyapunov metric This is a general construction when dealing with uniform hyperbolicity [3]. In the 1D case, for an uniformly attracting torus with transfer matrix M and Lyapunov multiplier λ, this metric is given by $|v|_\theta = S(\theta)|v|$, where $S : \mathbb{T} \to [1, \infty)$ is the continuous function

$$S(\theta) = \sum_{j=0}^{\infty} \frac{1}{\bar{\lambda}^j} |M(\theta + (j-1)\omega) \cdots M(\theta)|, \tag{12}$$

where $1 > \bar{\lambda} > |\lambda| + \varepsilon$, for sufficiently small $\varepsilon > 0$. Instead of considering this Lyapunov metric, we consider the transformations $P_1(\theta) = \frac{1}{S(\theta)}$ and $P_2(\theta) = S(\theta)$. Hence, we just define the continuous function

$$\Lambda(\theta) = P_2(\theta + \omega) M(\theta) P_1(\theta) = \operatorname{sgn}(M(\theta)) \left(\frac{S(\theta) - 1}{S(\theta)} \right) \bar{\lambda}, \tag{13}$$

where $\operatorname{sgn}(\cdot)$ is the sign function. Then, $|\Lambda(\theta)| < 1$ for all $\theta \in \mathbb{T}$.

Reducibility and almost reducibility to constant coefficients The goal of reducibility method is to reduce the transfer matrix to a constant Λ, which satisfies

$$M(\theta) P_1(\theta) = P_1(\theta + \omega) \Lambda, \tag{14}$$

for a suitable transformation P_1. If $M(\theta)$ is invertible for all $\theta \in \mathbb{T}$, this equation is solved by taking logarithms and solving the obtained small divisors equations by matching the Fourier coefficients.

If $M(\theta)$ has zeroes, equation (14) is not well-defined. Hence, we can not reduce $M(\theta)$ to constant coefficients. To overcome this difficulty, we consider the modified equation

$$(M(\theta)^2 + \varepsilon\eta(\theta))P_1(\theta)^2 = P_1(\theta+\omega)^2\lambda_\varepsilon^2, \tag{15}$$

for a suitable function $\eta\colon \mathbb{T} \to (0, +\infty)$ and a sufficiently small $\varepsilon > 0$.

One choice for the function η is $\eta(\theta) = 1 - \left(\dfrac{M(\theta)}{||M||_{\mathcal{C}^0}}\right)^2$. This function achieves its maximum value, 1, when the transfer matrix vanishes and decays rapidly outside its zeroes.

Notice that

$$\lambda_\varepsilon^2 = exp\left(\int_{\mathbb{T}} \log(M(\theta)^2 + \varepsilon\eta(\theta))d\theta\right), \tag{16}$$

hence we consider $\varepsilon > 0$ such that $\lambda_\varepsilon < 1$ (notice that $\lambda_0 < 1$).

By defining

$$\Lambda(\theta) = \frac{M(\theta)}{\sqrt{M(\theta)^2 + \varepsilon\eta(\theta)}}\lambda_\varepsilon \ ,$$

we obtain that $P_1, P_2 = P_1^{-1}$ and Λ satisfy equation

$$P_2(\theta+\omega)M(\theta)P_1(\theta) = \Lambda(\theta) \ .$$

Remark 5.1. *Even thought the analytical solution of small divisors equations involve the smoothness of the transfer matrix and diophantine properties of the rotation ω. In numerical computations these equations are solved by matching Fourier coefficients up to a finite order. These are intermediate computations to produce initial data to be validated by our computer programs. In fact, we give no proof about the reducibility properties of the transfer matrix.*

Numerical comparison of both methods The Lyapunov metric method and the almost reducibility method have been tested for the period 2 attracting curve of the quasiperiodically driven logistic map, with $D = 0.1$ and $a = 3.250$. In this case, the transfer matrix is noninvertible, hence nonreducible to constant. See figure 7 to check differences between both methods. Notice that the Fourier coefficients of the reduced matrix $\Lambda(\theta)$ decay slowly when using the Lyapunov metric method, while they decay exponentially fast when using the almost reducibility method.

5.3 Computer validations

We have validated the invariant curves appearing in the bifurcation diagram in figure 4(a), up to values of a close to the smooth bifurcations A-B (transcritical) and D-E (period doubling) and the non-smooth bifurcation E-F. We report here in detail the existence of the repellor in regions E and F, and the existence of the period 2 attracting curve near the non-smooth bifurcation E-F.

Invariant curves in regions A, B, C and D have been validated using no more than 20 Fourier modes. The validations near the smooth bifurcations have been performed obtaining results similar to the ones reported below for the repellor.

5.3.1 Validation of the repellor

Here we explain the validation of the repellor curve. First of all, we validate analytically the existence of this curve for $a \in (4.6, \infty)$ and then, via Computer Assisted Proofs, we validate it for $a \in (3.157065, 5)$ and check that the two families match.

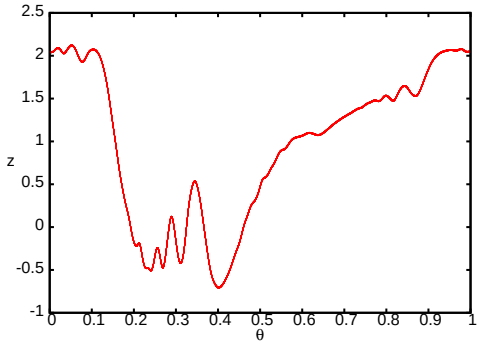

(a) Transfer matrix $M(\theta)$.

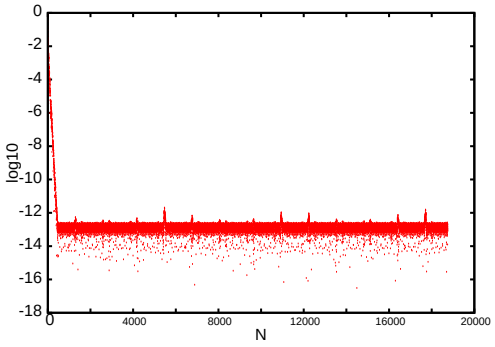

(b) Modes of the transfer matrix $M(\theta)$.

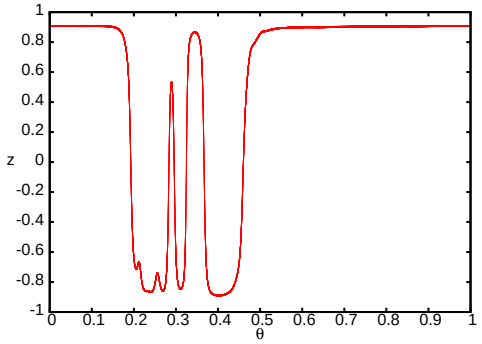

(c) Reduced matrix $\Lambda(\theta)$, computed via almost-reducibility method.

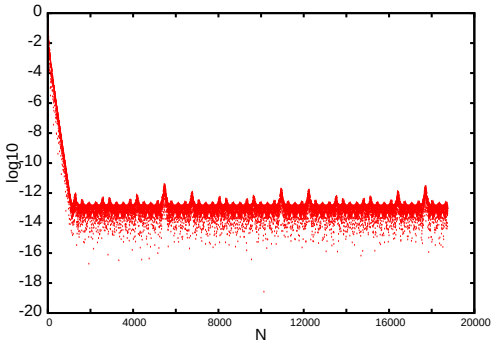

(d) Modes of the reduced matrix $\Lambda(\theta)$, computed via almost-reducibility method.

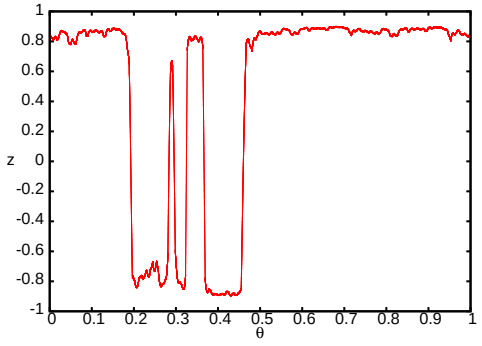

(e) Reduced matrix $\Lambda(\theta)$, computed via Lyapunov metric method.

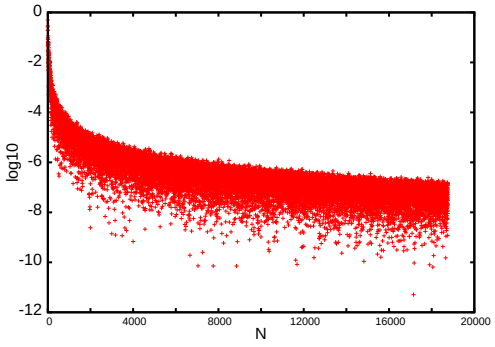

(f) Modes of the reduced matrix $\Lambda(\theta)$, computed via Lyapunov metric method.

Figure 7: Graphical comparison of the computed reduced $\Lambda(\theta)$ of the period 2 attracting curve, for $a = 3.25$ and $D = 0.1$.

Analytic validation For the analytic validation, it is convenient to consider the following right inverse of (F,ω):

$$\begin{array}{rccl}(G,\omega)\colon & \mathbb{R}\times\mathbb{T} & \longrightarrow & \mathbb{R}\times\mathbb{T}\\ & (z,\theta) & \longrightarrow & \left(\dfrac{1}{2}+\dfrac{1}{2}\sqrt{1-4\dfrac{z}{a(1+D\cos(2\pi(\theta-\omega)))}},\theta-\omega\right)\end{array}\ . \tag{17}$$

We apply the validation algorithm with the following initial data: $K(\theta)=\frac{a-1}{a}$, $P_1(\theta)=P_2(\theta)=1$, $\Lambda(\theta)=M(\theta)=\mathrm{D}_zG\left(\frac{a-1}{a},\theta\right)$. In the following, we consider the bound

$$\Delta=\sqrt{1-\frac{4(a-1)}{a^2(1-D)}}\ .$$

The constants $\rho=\frac{1}{2}-\frac{1}{a}-\frac{1}{2}\Delta$, $\sigma=\tau=0$ and $\lambda=\hat{\lambda}=\frac{1}{a(1-D)\Delta}$ satisfy inequalities 2.1), 2.2), 2.3), 2.4) of the validation theorem 2.4. Inequality 2.5) is satisfied if $a>\frac{1}{(1-D)\Delta}$.

Choosing $r=\frac{2\rho}{1-\lambda}$, we obtain the upper bound of the second derivative 3.1) to be

$$b=\frac{2}{a^2(1-D)^2\left(1-\frac{4\left(\frac{a-1}{a}+r\right)}{a(1-D)}\right)^{\frac{3}{2}}}\ ,$$

from which we obtain $h=(1-\lambda)^{-2}b\rho$. Fix D, for $a>0$ sufficiently big, we obtain $h<\frac{1}{2}$ and then there is a unique invariant torus close to initial data K. In particular, for $D=0.1$, we obtain the crude lower bound $a>4.6$ (for which $h<0.45$).

Computer validation After we have shown the existence of the repellor curve for values $a>4.6$, we have proved (computer assisted) the existence of the family of the repellor curve for $3.157065\leq a\leq 5$, starting at $a=5$. This validation has been done, using expression (11), by computing the initial data using the algorithms exposed in subsection §5.2 with 30 Fourier modes. We emphasize that the width of the intervals of validation shorten as they approach to the period doubling bifurcation value $a\simeq 3.143$. The algorithm stops when the width of the intervals is less that 10^{-6}, reaching $a=3.157065$. See figure 8(a).

Remark 5.2. *The algorithm stops at a distance* $1.5\cdot 10^{-2}$ *of the predicted bifurcation value because the Lyapunov multiplier (bounded by* λ*) of the invariant curve decreases goes to* 1.

Remark 5.3. *In this computation we have applied 2800 times the validation algorithm and the time of computation has been around 307 minutes. This means that each validation step, which consists in computing the initial data, validating the existence and uniqueness of a FHIT near it, and then, checking the matching, has spent around 6.5 seconds.*

In order to show how the upper bounds of the validation algorithm behave near the bifurcation value, we have applied the validation algorithm for values $a=3.16+0.01\cdot j$, with $j=0,\ldots,184$, using 30 Fourier modes. The results are displayed in figures 8(b), 8(c) and 8(d).

Remark 5.4. *It is remarkable that, although the validations are done using a library that operates with intervals in* `double` *precision, the errors can achieve order* 10^{-10}.

5.3.2 Validation of the period 2 attracting curve

The goal in this subsection is to validate period 2 attracting curves near the predicted non-smooth bifurcation value $a_*\approx 3.271$. To do so, we have considered the 2 times composition of the driven logistic map (11):

$$\begin{array}{rccl}(F,\omega)^2\colon & \mathbb{R}\times\mathbb{T} & \longrightarrow & \mathbb{R}\times\mathbb{T}\\ & (z,\theta) & \longrightarrow & (F(F(z,\theta),\theta+\omega),\theta+2\omega)\end{array}\ . \tag{18}$$

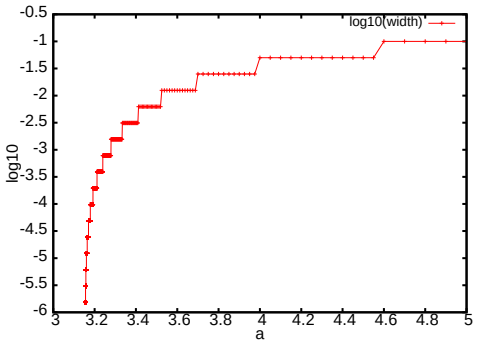

(a) Width of the intervals of the family validation.

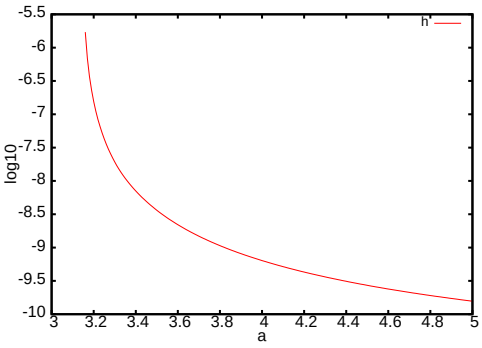

(b) h value of the validations.

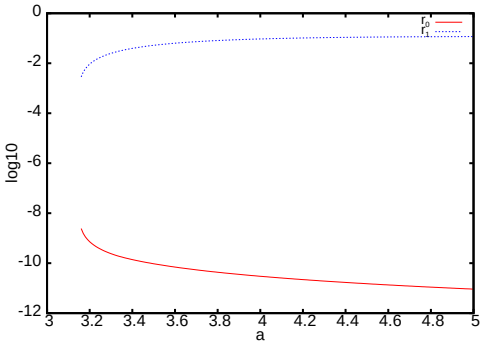

(c) r_0 and r_1 values of the validations.

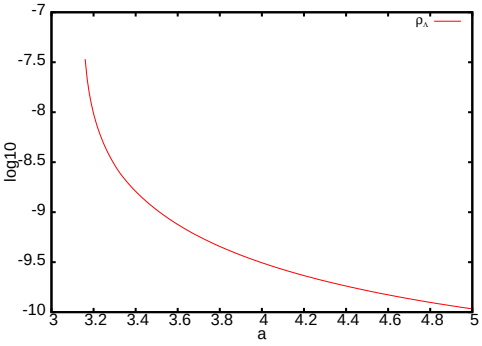

(d) ρ_Λ error values.

Figure 8: Data obtained of the validations of the repellor curve for $D = 0.1$.

First, we have performed a numerical study of the regularity of the initial data: the torus K, the transformations P_1 and P_2, and the normalized cocycle Λ. Since the associated transfer matrix M is noninvertible, we have used the almost-reducibility method to compute P_1, P_2 and Λ. In figure 9, it is shown, with respect to a, a numerical estimate of the maximum slope of the computed initial data. Note that P_1 is the initial data that has the biggest slope. For example, at $a = 3.265$ the slope of P_1 is $4.3 \cdot 10^4$, while the slopes of the torus and the normalized cocycle are $2.4 \cdot 10^1$ and $3.07 \cdot 10^3$, respectively. Notably, at $a = 3.269$ the slope of P_1 is $4.25 \cdot 10^6$. Hence, P_1 is used in order to determine the number of Fourier modes in the validation process. In figure 10, it is shown the initial data K (and M), P_1 and Λ for $a = 3.265$ and $a = 3.269$. Notice that a small change of the value of a leads to a dramatic change of the initial data.

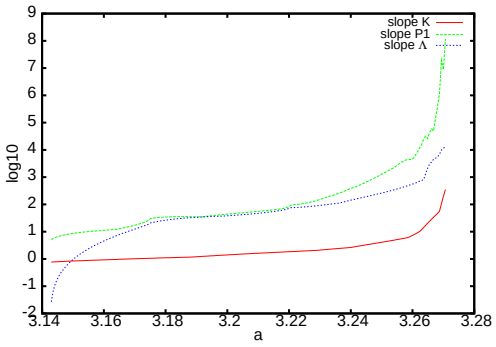

Figure 9: Maximum slopes of the period 2 attracting curve K (in red), its P_1 transformation (in green) and the normalized cocycle Λ (in blue), with respect to parameter a.

The validation results for different values of the parameter a are shown in table 3. Note that in all these validations is that the time computation depends heavily on the regularity of the initial data.

a	3.265	3.268	3.269
h	3.046383e-05	2.248226e-03	4.203495e-01
r_0	5.365990e-09	1.701127e-07	3.635973e-06
ρ_Λ	5.815762e-03	4.542701e-04	-
order	3000	17000	27000
time (minutes)	5	130	361

Table 3: Validation results of the period 2 invariant torus of the driven logistic map for different values of a close to breakdown.

6 Final comments

The main message of this paper is that good numerics lead to successful validations. Notably, the knowledge of the dynamics around the torus is an important ingredient for an accurate numerical computation.

The computational time of the validation algorithms depends primarily on the regularity of the initial data, and hence, their number of Fourier modes. The most expensive computations with Fourier models are the product and the evaluation. Although the times reported in this paper correspond to computations with a single processor, we have also used the library `OpenMP` (see [7]) in order to have parallel computations (by distributing the product and evaluation routines on the processors).

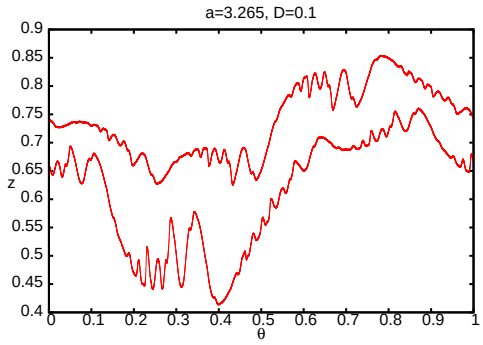

(a) Tori $K(\theta)$ and its image, for $a = 3.265$.

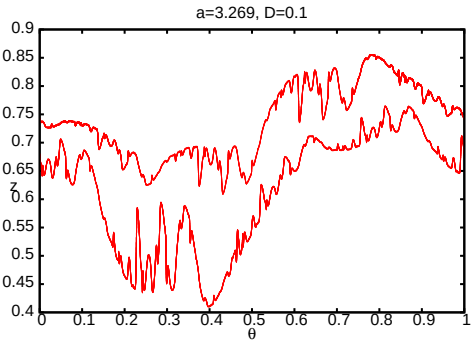

(b) Tori $K(\theta)$ and its image, for $a = 3.269$.

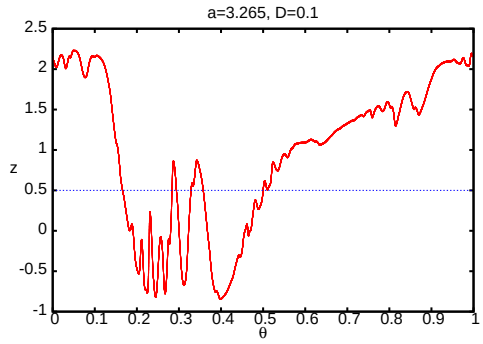

(c) Cocycle $M(\theta)$, for $a = 3.265$.

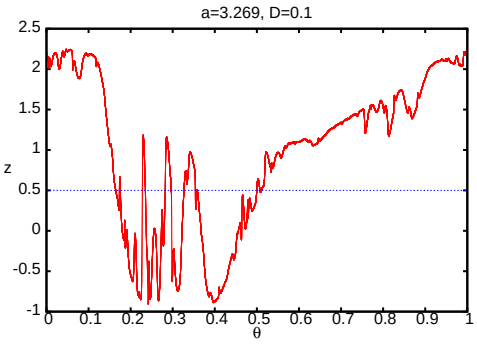

(d) Cocycle $M(\theta)$, for $a = 3.269$.

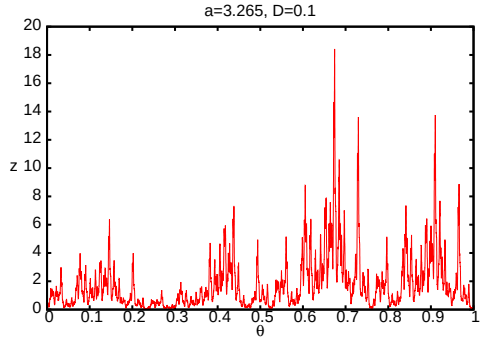

(e) Transformation $P_1(\theta)$, for $a = 3.265$.

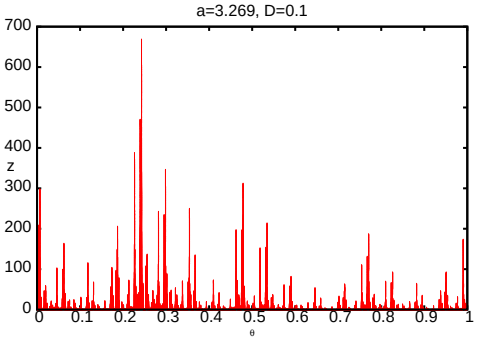

(f) Transformation $P_1(\theta)$, for $a = 3.269$.

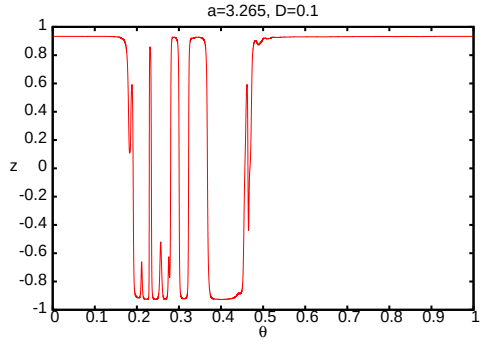

(g) Reduced cocycle $\Lambda(\theta)$, for $a = 3.265$.

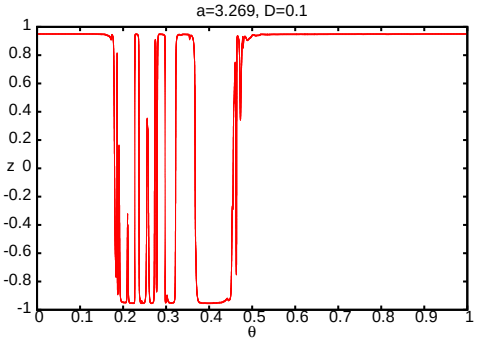

(h) Reduced cocycle $\Lambda(\theta)$, for $a = 3.269$.

Figure 10: Graphs of the initial data close to the breakdown of the period 2 curve.

The models worked out in this paper have simple analytic expressions. But our validation algorithms can be applied to more general models, as long as we are capable of evaluating the map (and its first and second derivatives). For instance, for a skew product flow, we can consider its Poincaré map [4, 31]. In these general cases, we substitute the Fourier arithmetics by the upper bounds of the validation theorem. Nevertheless, in the examples of this paper this methodology is not as accurate, especially in the extreme cases we consider. For instance, in the Heagy-Hammel fractalization route, for $a = 3.265$, the validation of the period 2 attracting curve has been performed with 3000 Fourier modes. While the direct evaluation method needs about 1255319 interval subdivisions of $[0, 1]$ in order to achieve the same accurate results.

Acknowledgments

We thank Angel Jorba, Rafael de la Llave and Carles Simó for their comments and fruitful discussions on different aspects of this research. We thank Alejandra Gonzalez and Pere Gomis for proofreading a former version of this paper. We further thank the developers of the rigorous interval library `filib++`.

References

[1] R. A. Adomaitis and I. G. Kevrekidis. Noninvertibility and the structure of basins of attraction in a model adaptive control system. *J. Nonlinear Sci.*, 1(1):95–105, 1991.

[2] R. A. Adomaitis, I. G. Kevrekidis, and R. de la Llave. A computer-assisted study of global dynamic transitions for a noninvertible system. *Internat. J. Bifur. Chaos Appl. Sci. Engrg.*, 17(4):1305–1321, 2007.

[3] D. V. Anosov. *Geodesic flows on closed Riemann manifolds with negative curvature.* Proceedings of the Steklov Institute of Mathematics, No. 90 (1967). Translated from the Russian by S. Feder. American Mathematical Society, Providence, R.I., 1969.

[4] M. Berz and K. Makino. Verified integration of ODEs and flows using differential algebraic methods on high-order Taylor models. *Reliab. Comput.*, 4(4):361–369, 1998.

[5] M. J. Capiński. Covering relations and the existence of topologically normally hyperbolic invariant sets. *Discrete Contin. Dyn. Syst.*, 23(3):705–725, 2009.

[6] Alessandra Celletti and Luigi Chierchia. KAM stability and celestial mechanics. *Mem. Amer. Math. Soc.*, 187(878):viii+134, 2007.

[7] B. Chapman, G. Jost, and R. van der Pas. *Using OpenMP: Portable Shared Memory Parallel Programming (Scientific and Engineering Computation).* The MIT Press, October 2007.

[8] R. de la Llave. Hyperbolic dynamical systems and generation of magnetic fields by perfectly conducting fluids. *Geophys. Astrophys. Fluid Dynam.*, 73(1-4):123–131, 1993. Magnetohydrodynamic stability and dynamos (Chicago, IL, 1992).

[9] R. de la Llave and D. Rana. Accurate strategies for K.A.M. bounds and their implementation. In *Computer aided proofs in analysis (Cincinnati, OH, 1989)*, volume 28 of *IMA Vol. Math. Appl.*, pages 127–146. Springer, New York, 1991.

[10] R. de la Llave and David Rana. Accurate strategies for small divisor problems. *Bull. Amer. Math. Soc. (N.S.)*, 22(1):85–90, 1990.

[11] N. Fenichel. Persistence and smoothness of invariant manifolds for flows. *Indiana Univ. Math. J.*, 21:193–226, 1971/1972.

[12] A. Haro and R. de la Llave. Manifolds on the verge of a hyperbolicity breakdown. *Chaos*, 16(1):013120, 8, 2006.

[13] A. Haro and R. de la Llave. A parameterization method for the computation of invariant tori and their whiskers in quasi-periodic maps: numerical algorithms. *Discrete Contin. Dyn. Syst. Ser. B*, 6(6):1261–1300 (electronic), 2006.

[14] A. Haro and R. de la Llave. A parameterization method for the computation of invariant tori and their whiskers in quasi-periodic maps: rigorous results. *J. Differential Equations*, 228(2):530–579, 2006.

[15] A. Haro and R. de la Llave. A parameterization method for the computation of invariant tori and their whiskers in quasi-periodic maps: explorations and mechanisms for the breakdown of hyperbolicity. *SIAM J. Appl. Dyn. Syst.*, 6(1):142–207 (electronic), 2007.

[16] A. Haro and J. Puig. Strange nonchaotic attractors in Harper maps. *Chaos*, 16(3):033127, 7, 2006.

[17] J. F. Heagy and S. M. Hammel. The birth of strange nonchaotic attractors. *Phys. D*, 70(1-2):140–153, 1994.

[18] M. W. Hirsch, C. C. Pugh, and M. Shub. *Invariant manifolds*. Lecture Notes in Mathematics, Vol. 583. Springer-Verlag, Berlin, 1977.

[19] A. Jorba and J. C. Tatjer. A mechanism for the fractalization of invariant curves in quasi-periodically forced 1-D maps. *Discrete Contin. Dyn. Syst. Ser. B*, 10(2-3):537–567, 2008.

[20] J. A. Ketoja and I. I. Satija. Harper equation, the dissipative standard map and strange nonchaotic attractors: relationship between an eigenvalue problem and iterated maps. *Phys. D*, 109(1-2):70–80, 1997. Physics and dynamics between chaos, order, and noise (Berlin, 1996).

[21] H. Koch. A renormalization group fixed point associated with the breakup of golden invariant tori. *Discrete Contin. Dyn. Syst.*, 11(4):881–909, 2004.

[22] H. Koch. Existence of critical invariant tori. *Ergodic Theory Dynam. Systems*, 28(6):1879–1894, 2008.

[23] Yu. D. Latushkin and A. M. Stëpin. Weighted shift operators, the spectral theory of linear extensions and a multiplicative ergodic theorem. *Mat. Sb.*, 181(6):723–742, 1990.

[24] M. Lerch, G. Tischler, J. W. Von Gudenberg, W. Hofschuster, and W. Krämer. Filib++, a fast interval library supporting containment computations. *ACM Trans. Math. Softw.*, 32(2):299–324, 2006.

[25] Ugo Locatelli and Antonio Giorgilli. Invariant tori in the Sun-Jupiter-Saturn system. *Discrete Contin. Dyn. Syst. Ser. B*, 7(2):377–398 (electronic), 2007.

[26] R. Mañé. Persistent manifolds are normally hyperbolic. *Trans. Amer. Math. Soc.*, 246:261–283, 1978.

[27] J. N. Mather. Characterization of Anosov diffeomorphisms. *Nederl. Akad. Wetensch. Proc. Ser. A 71 = Indag. Math.*, 30:479–483, 1968.

[28] R. E. Moore. *Interval analysis*. Prentice-Hall Inc., Englewood Cliffs, N.J., 1966.

[29] N. Revol, K. Makino, and M. Berz. Taylor models and floating-point arithmetic: proof that arithmetic operations are validated in cosy. *Journal of Logic and Algebraic Programming*, 64(1):135 – 154, 2005.

[30] R. J. Sacker and G. R. Sell. Existence of dichotomies and invariant splittings for linear differential systems. I. *J. Differential Equations*, 15:429–458, 1974.

[31] D. Wilczak and P. Zgliczyński. c^r-lohner algorithm. `arXiv:0704.0720v1`, 2007.

[32] P. Zgliczyński and M. Gidea. Covering relations for multidimensional dynamical systems. *J. Differential Equations*, 202(1):32–58, 2004.